A Characterization of the Meteorological Environment Associated with the Tropical Transition of a Medicane in the Western Mediterranean Sea

Edoardo Mazza*, Uwe Ulbrich† and Rupert Klein‡

*Corresponding author address: Institute of Meteorology, Freie Universität, Carl-Heinrich-Becker-Weg 6-10, 12165 Berlin, Germany.

E-mail: edoardo.mazza@met.fu-berlin.de

†Current affiliation: Institute of Meteorology, Freie Universität, Carl-Heinrich-Becker-Weg 6-10, 12165 Berlin, Germany.

‡Current affiliation: Institute of Mathematics, Freie Universität, Arnimallee 6, 14195 Berlin, Germany.

ABSTRACT

In order to identify the distinctive characteristics of the meteorological environment supporting the tropical transition of the October 1996 medicane in the western Mediterranean, its spatial and temporal evolution is investigated on the basis of a 50-member ensemble of reanalyses-driven RCM atmospheric simulations. As the cyclones undergo a warm seclusion-like process, the initial thermal asymmetries and vertical tilt are reduced while a warm core builds upward from the lower troposphere. A comparison of the composite environments of transitioning and non-transitioning storms reveals that the former feature enhanced convection and higher mid-to-low tropospheric relative humidity, resulting in a stronger diabatic heat release aloft, along with increased upper-level wind divergence. At the time of transition, vertical wind shear is not significantly different, as it is reduced in both composites below the thresholds typically found for tropical cyclogeneses. Upper-level wind divergence and wind shear are positively correlated, hence the additional forcing on convection due to stronger divergence could partially counteract the detrimental effects of larger shear. In the transitioning cyclones, surface sensible and latent heat fluxes become significantly larger only in proximity of the transition. Finally, the upper-tropospheric warm core strength exhibits a strong, negative linear correlation with wind shear. Moderately positive correlation coefficients are instead found for latent and sensible heat fluxes while upper-level divergence and mid-to-low tropospheric relative humidity show small and negative correlations.

1. Introduction

Over the last years there has been a remarkable advance in our understanding of both mid-latitude and tropical cyclones: used to be grouped in separate classes, they are now rather envisioned at each end of a continuum spectrum where, based on its location and meteorological environment, a cyclone can acquire distinctive characteristics of each class (Hart 2003). For example, during *extratropical transitions* tropical cyclones (TCs) usually move to higher latitudes and undergo a series of structural changes resulting in the acquisition of features typical of baroclinic systems (Jones et al. 2003). Conversely, a *tropical transition* refers to the formation of a TC from a well-defined baroclinic precursor or remnant baroclinic structure (Bosart and Bartlo 1991; Davis and Bosart 2003, 2004). McTaggart-Cowan et al. (2012) estimated that baroclinic influences account for nearly 30 % of the global tropical cyclogeneses and there is increasing evidence that the tropical transition paradigm can be applied to understand the genesis of *medicanes* or *tropical-like cyclones* in the Mediterranean Basin as well (McTaggart-Cowan et al. 2009a,b; Chaboureau et al. 2012).

Although forming in a highly cyclogenetic area (Trigo et al. 1999), only 1.6 $\pm$ 1.3 medicanes are detected on average every year (Cavicchia et al. 2014). The synoptic setting associated with their genesis is often characterized by an upper-level feature (Claud et al. 2010), either a fully isolated cut-off (Reale and Atlas 2001) or an elongated trough (Pantillon et al. 2012), responsible for the destabilization of the atmospheric column (Emanuel 2005; Fita et al. 2007; Cavicchia et al. 2014) and the quasi-geostrophic forcing on vertical motions (Chaboureau et al. 2012). In the lower troposphere, instead, enhanced vorticity is present (Cavicchia et al. 2014) along with consistent heat fluxes from the sea surface (Pytharoulis et al. 2000; Reale and Atlas 2001).

Through observations and numerical modeling, several studies have investigated the relevance of different processes in the evolution of medicanes. Surface heat fluxes appear to be involved not only in maintaining the systems (Fita et al. 2007; Davolio et al. 2009; Lagouvardos et al. 1999; Pytharoulis et al. 2000; Moscatello et al. 2008b) but also in promoting the scale reduction of the vortex (Reed et al. 2001) and in modifying the stability of the boundary layer (Moscatello et al. 2008a). Diabatic effects, such as latent heat release by condensation, control medicanes' intensification (Pytharoulis et al. 2000) as the strongest convective activity is found before the storms' maturity (Chaboureau et al. 2012; Miglietta et al. 2013). In terms of the dynamics, the interplay between a coherent tropopause disturbance, a diabatically-generated potential vorticity (PV) anomaly and an orographically-generated PV banner was identified by McTaggart-Cowan et al. (2009a,b) as the key mechanism in the cyclogenesis of a medicane in the Gulf of Genoa. Chaboureau et al. (2012) pointed instead to the enhancement in convection due to the surface cyclone crossing an upper-level jet as a major contributor to the tropical transition of the September 2006 medicane.

Tous and Romero (2011, 2013) used reanalysis data to investigate the meteorological environment associated with twelve medicanes by comparing it against that of the bulk of the Mediterranean cyclones. Among the parameters examined, only heat fluxes, expressed as a diabatic contribution to surface equivalent potential temperature, and an empirically-defined genesis index proved to be moderately distinctive. An axisymmetric, cloud-resolving model was instead employed by Fita et al. (2007) to show that medicanes are highly sensitive to the relative humidity (RH) profile while less sensitive to the sea surface temperature (SST), as also suggested by Tous et al. (2013), even though a lower limit of 15° C seems necessary for their genesis (Tous and Romero 2013). The geographical and seasonal frequency of medicane genesis is compatible to that of the combination of low wind shear, large thermal contrast between the upper troposphere and the sea surface, high column-integrated relative humidity and large low-level vorticity, according to Cavicchia et al. (2014).

Our present study attempts at characterizing the meteorological environment associated with the tropical transition of medicanes by focusing on the October 1996 event. In order to do so, an ensemble of model realizations is obtained through a dynamical downscaling of the corresponding, reanalysis-based, synoptic scale environment. This approach differs from previous studies in that it is based on the spatio-temporal comparison of transitioning and non-transitioning ensemble members. Moreover, the use of a full-physics, non-hydrostatic atmospheric model should allow a better representation of any baroclinic influence that an axisymmetric model initialized with a homogenous atmosphere can not account for, as suggested by Fita et al. (2007). The analysis focuses on different parameters that have been often investigated in relation to extratropical and tropical cyclones, namely vertical wind shear, upper-tropospheric wind divergence, surface heat fluxes and relative humidity. The results are discussed with respect to similar studies on medicanes, TCs as well as on the baroclinically-induced pathway (i.e. tropical transition) to TC formation.

The remainder of the paper is organized as follows: section 2 provides the case overview, section 3 describes the model set up and the methodology, in section 4 the results are presented. The discussion and concluding remarks are included in section 5.

2. Case description

The October 1996 medicane is among the twelve cases detected by Tous and Romero (2011) and was previously investigated by Reale and Atlas (2001) and Cavicchia and von Storch (2012). Its precursor cyclone originated off the Algerian coast in the afternoon of 6 October and was initially located under an upper level, cut-off low, associated with a moderately strong jet stream on its southern edge (Reale and Atlas 2001), that moved from southern France to the Catalan Coast. It later progressed northward between Sardinia and the Balearic Islands (Fig.1a) and by 1200 UTC 7 October it featured a 999 hPa sea-level pressure minimum, an incipient low-level warm core and a well-defined, eye-like structure (Reale and Atlas, 2001). Subsequently, the system made its first landfall over southern Sardinia (Cavicchia and von Storch 2012), temporarily weakening and partially losing its tropical-like structure (Fig.1b). Soon after 00 UTC 8 October, the cyclone moved over the Tyrrhenian Sea regaining strength and the eye-like structure (Fig.1c). According to Reale and Atlas (2001) and Cavicchia and von Storch (2012) a ship located around 100 km off the center recorded winds up to 25 m/s. On 9 October, the system moved south-eastward with wind speeds reaching 22.5 m/s on the island of Ustica. Having traveled almost 3000 km (Cavicchia and von Storch 2012), the medicane dissipated after making landfall over Calabria on 10 October 1996 (Fig.1d). The 0.6 μm visible channel imagery in Fig.1 provides also indications of the baroclinic-like characters of its precursor cyclone (Fig.1a), such as remnant frontal structures, as well as evidence of the axisymmetrization of the cloud pattern around the eye and the scale reduction of the vortex during tropical transition (Fig.1b and Fig.1c).

3. Data and methodology

a. Experimental set-up

The numerical simulations are performed with the full physics, non-hydrostatic, limited area model COSMO-CLM (Rockel et al. 2008) version $cosmo4.8-clm19$ in a double, one-way nested configuration. A 288x192 points, 0.0625°resolution grid is nested in a 257x271 points, 0.165°resolution grid. In both settings, 40 vertical levels are used and lateral boundary conditions are updated every 6 hours. For the inner grid the chosen set-up consists of: the extended Kessler−type mycrophysics scheme, including cloud water and cloud ice for grid-scale precipitation, the Ritter and Geleyen radiation scheme and the Tiedtke convection parametrization scheme (Tiedtke 1989). The horizontal diffusion parameters are modified according to Akhtar et al. (2014). Two sets of simulations are performed with initial and boundary conditions provided by the 1.125° resolution version of the ERA−40 reanalysis (Uppala et al. 2005) and the 0.7° resolution ERA Interim reanalysis (Dee et al. 2011) respectively.

b. Ensemble generation

Indications exist that forecasts of medicanes are highly sensitive to the initial conditions (Davolio et al. 2009; Chaboureau et al. 2012), therefore a simple technique, referred to as *domain shifting* (DS), is here employed to generate a set of initial conditions for the ensemble of model simulations. DS consists of performing the numerical integrations over domains that cover a common area of interest but are shifted with respect to each other. A simplified representation of the modeling scheme is provided in Fig.2. The procedure is applied to the first downscaling step of reanalysis as follows:

- A central domain (ORIG - centered on 9.75°W, 49.68°N) is located (black box in Fig.2).
- Select the shifting distances: 68 km, 136 km and 184 km.
- Shift the central domain by each distance in cardinal and primary inter-cardinal directions (e.g. North and North-West), obtaining a total of 25 different domains.
- Run the atmospheric simulation for each of the domains.

Using two reanalyses as driving data results in 50 simulations, each of them further downscaled to 0.0625° over a common nested domain covering the western and central Mediterranean (magenta box in Fig.2). The simulations are initialized at 00 UTC 1 October 1996 for the first downscaling and at 00 UTC 4 October 1996 for the second one.

c. Cyclone Phase Space

The tropical transition of the simulated cyclones is are assessed by means of the Hart's cyclone phase space (Hart 2003): a three dimensional diagnostic methodology that has already been applied to the study of medicanes (see Davolio et al. 2009; Cavicchia and von Storch 2012; Miglietta et al. 2013). The parameters that define the phase space are:

- The thermal symmetry in the lower troposphere (B): the difference in storm-relative 600-900 hPa thickness between left and right semicircles with respect to the current cyclone's motion.
- The lower tropospheric thermal wind (-V_T^L): the vertical derivative of the cyclone's height perturbation between 900 and 600 hPa.
- The upper tropospheric thermal wind (-V_T^U): the vertical derivative of the cyclone's height perturbation between 600 and 300 hPa.

Due to the smaller scale of medicanes, these are calculated within a 300 km radius around the SLP minimum, instead of the 500 km one used for TCs by Hart (2003). Nevertheless, consistent results are obtained for radii ranging between 150 and 350 km. In our application, a cyclone is said to be a medicane when it completes the tropical transition, meeting simultaneously all of three requirements imposed by Hart (2003): B $<$ 10 m, -V_T^L >0 and -V_T^U >0. The first hourly time step in which all the conditions are met is termed Tropical Transition time (TT). For the non-transitioning cyclones, the TT time is taken to be the time of maximum upper-tropospheric warm core strength (-V_T^U) provided that the other two conditions are met.

d. Cyclone Composites

Previous studies concluded that horizontal resolutions in the order of 7 km are appropriate for correctly simulating sub-synoptic scale cyclones such as medicanes (Tous and Romero 2013;

Miglietta et al. 2013). Therefore, the analysis is entirely based on the results of the 0.0625° resolution simulations as obtained from the second downscaling. Two methods are employed to minimize the effect of the vortex's symmetric circulation on the values of wind shear: for the spatial plots, it is calculated after having low-pass filtered the u and v fields via convolution with a 21x21 gridpoint filter; for the time series, it is calculated as the difference in the composite area-averaged wind vectors between 300 and 850 hPa, similarly to the method of Paterson et al. (2005)

Cyclone compositing has been frequently applied to the study of extratropical and tropical cyclones (see Frank 1977; Bracken and Bosart 2000; Bengtsson et al. 2007; Catto et al. 2010) in order to retain only those features that appear consistently in a given dataset. It is here implemented as follows: each simulated cyclone is tracked using sea-level pressure (SLP) fields, requiring the associated minimum to be deeper than 1013 hPa. Subsequently, cyclone-centered hourly fields are composited over a 280x280 km regular grid. The 0-hour offset is placed on the TT time and composites are obtained in the time range from TT-12h to TT+12h. Given the similarity of the storm tracks in the ensemble and the absence of relevant grid stretching due to the limited size of the domain, the compositing procedure does not include any additional spatial transformation. Two composites are built: *MED* for the medicanes and *NONMED* for the non-transitioning cyclones.

The statistical significance of the composite difference (MED-NONMED), standardized by the 50-member standard deviation, is tested at the 95% confidence interval by means of a bootstrapping by resampling approach as in (Rios-Berrios et al. 2015), by randomly replacing composite members. Using this method, the significance is tested both for individual grid point values and area-averaged quantities without assuming a specific probability distribution for the variables in the ensemble.

4. Results

a. Evolution of the composites

According to the phase space metrics, all the simulated 50 cyclones attain a state characterized by negligible thermal asymmetry (B $<$ 10 m) and a warm core in the lower troposphere (-V_T^L >0), as seen in Fig.3a. Among these, only 27 cyclones exhibit a warm core also in the upper troposphere (-V_T^U >0 - red markers in Fig.3b) and are identified as medicanes. For the remaining 23 non-transitioning cyclones, -V_T^U never exceeds 0 (blue markers in Fig.3b). In both composites, the warm core formation appears to follow a bottom-up evolution: as the SLP minimum deepens (solid lines in Fig.3c) a low-level warm anomaly develops, indicated by the positive -V_T^L values (solid lines with circular markers) in Fig.3c. As shown in the 900 hPa potential temperature fields in Fig.4a, this thermal anomaly is located at the end of a bent-back warm front. This development is reminiscent of warm seclusions and the stage 3 of the Shapiro and Keyser (1990) marine cyclone model.

The baroclinic origin of the cyclones is clearly visible in the longitudinal cross sections through the composites' centers (Fig.4b): both in MED and NONMED an upper level, geopotential height anomaly (calculated as the difference from the zonal mean) encroaches on a near-surface horizontal equivalent potential temperature gradient. In such a structure, the advection of cyclonic vorticity by the thermal wind would promote upward vertical motions. During the seclusion, the low-level asymmetry and the vertical tilt are reduced as the upper-level anomaly weakens. A similar pathway has already been documented in several tropical transitions of Atlantic hurricanes (Hulme and Martin 2006, 2009a,b).

Although the composites follow a very similar evolution, there exist remarkable differences in the associated convective activity, both in terms of intensity and location. At 500 hPa, the MED composite has stronger convection with peaks closer to the composite center (Fig.5a). Larger, positive vertical velocities are present in the transitioning cyclones throughout the troposphere, with the largest difference located between 400-600 hPa (Fig.5b) over much of the period preceding the TT. Such stronger convection contributes to a more intense warming in the mid-troposphere: significantly larger latent heat release is in fact present between 400 and 700 hPa (Fig.5b). This is consistent with the greater SLP fall seen in the MED composite and the subsequent formation of the 300-600 hPa warm core, lagging approximately 6 hours behind the lower tropospheric one (Fig.3c).

b. Shear and divergence

Vertical wind shear is believed to have detrimental effects on TCs (McBride and Zehr 1981; DeMaria et al. 2001; Gallina and Velden 2002) as well as on medicanes (Reale and Atlas 2001; Tous and Romero 2013). The time series of 300-850 hPa wind shear for MED and NONMED are shown in Fig.6a. During tropical transitions a marked shear reduction is generally observed (Davis and Bosart 2004; Hulme and Martin 2009a,b). In both composites the shear decreases from values exceeding 15 m/s to less than 6 m/s at the TT, however in the transitioning cyclones it reamins significantly stronger until TT-3 hours. As shown in Fig.7a, the largest difference, standardized by the ensemble standard deviation, exceeds 1 σ and is located to the north-west of the composite center. Conversely from previous studies (Davis and Bosart 2003; Kaplan et al. 2010) even in the non-transitioning storms the shear weakens on average below 10 $\mathrm{m/s}$. In the MED composite, however, this reduction is more pronounced. Hulme and Martin (2009a,b) emphasized the role of diabatic processes in reducing the vertical wind shear through a redistribution of PV.

Upper-level wind divergence can provide the forcing necessary to support convection during a tropical transition (Chaboureau et al. 2012): for a 5-hour period extending for TT-4 to TT+1, the transitioning cyclones are characterized on average by a significantly larger divergence at 300 hPa (Fig.6b). As shown in Fig.7b, there is a well-defined divergence maximum to the north-west of the cyclones center, whose amplitude exceeds 6x10^{-5} 1/s, in agreement with the NCEP analyses presented by Reale and Atlas (2001). Associated with it, an extensive area of significanty larger divergence characterizes the MED composite as soon as TT-8 hours and persists throughout the transition process.

The scatter plot in Fig.6c indicates that in both composites tropospheric wind shear and upper-level divergence are positively correlated: a linear fit between their respective area-averaged, hourly values for each composite member yields very similar positive slopes (1.45x10^{-5} and 1.51x10^{-5}) and correlation coefficients of 0.37 and 0.4 respectively. Such compensation could partially counteract the detrimental effects of the enhanced wind shear observed in the MED composite by providing an additional forcing on convection, as suggested by Hendricks et al. (2010) for rapidly intensifying TCs.

c. Heat Fluxes and Humidity

Medicanes obtain their energy from the thermodynamical disequilibrium between the atmosphere and the sea surface (Emanuel 2005; Fita et al. 2007; Tous and Romero 2013): heat fluxes from the sea can support their intensification through the so-called Wind Induced Surface Heat Exchange (WISHE) mechanism (Emanuel 1986; Rotunno and Emanuel 1987), according to Emanuel (2005) and Fita et al. (2007). As shown by the time series in Fig.8a,b, latent and sensible heat fluxes become significantly stronger in the MED composite only in proximity of the transition, with anomalies that at TT+6 hours exceed 60 W/m^2 and 30 W/m^2 respectively. This result questions a causal relationship between heat fluxes and the tropical transition. Conversely, the evidence seems to support latent and sensible heat fluxes as factors contributing to medicanes' intensification after the storms reached a sufficient strength and axisymmetric structure, as Davis and Bosart (2003) indicated in the case of baroclinically-induced TCs.

Relative humidity has often been investigated in relation to tropical cyclogeneses (see Hendricks et al. 2010; Wu et al. 2012; Brown and Hakim 2015). Different measures of RH have been used to assess its role in medicanes formation: Tous and Romero (2013) focused on its value at the 600 hPa level while Fita et al. (2007) and Cavicchia et al. (2014) considered vertically-integrated RH. Nevertheless, medicanes appear to be associated with a very humid atmospheric column. Fig.5b shows that the MED composite is more humid across a vast part of the troposphere, with the greatest differences with respect to NONMED located in between 600 and 850 hPa. The time series in Fig.9a shows that the 600-850 hPa mean relative humidity presents a significantly positive anomaly across the entire 25-hour period, with peaks exceeding 5%. Spatially, the anomaly covers a large portion of the composite area and wraps cyclonically around the center (Fig.9b). It is characterized by azimuthal asymmetries throughout the transition process and by local maxima exceeding 1.5/2 σ.

d. Influence on warm core formation

So far, the analysis focused on describing the differences between the average meteorological environments of transitioning and non-transitioning storms. To better understand how these might influence the genesis of medicanes, i.e. the formation of a full tropospheric warm core, the relationship between each of the examined variables and the upper-tropospheric warm core metric of the cyclone phase space ($-V_T^U$) is examined. The scatter plots of hourly, area-averaged values for each composite member reveal a strong, negative linear correlation between the tropospheric wind shear and the warm core strength, with Pearson correlation coefficients of -0.88 and -0.7 for MED and NONMED respectively (Fig.10a) . Negative but smaller correlation coefficients are also found for 300 hPa wind divergence (Fig.10b). There appears to be instead a moderately strong positive correlation between latent heat flux and warm core strength, with a coefficients equal to 0.58 for MED and 0.43 for NONMED (Fig.10c), even though medicanes were not characterized by larger heat fluxes before TT. Very similar findings hold also for the sensible heat flux (not shown). Conversely, despite the MED composite time series exhibiting a consistently significant and positive anomaly, the correlation of mid-tropospheric relative humidity and warm-core strength is weak and negative (Fig.10d).

5. Discussion

This study aims at characterizing the meteorological environment supporting the tropical transition of the October 1996 medicane by comparing the composite environments of 27 transitioning and 23 non-transitioning cyclones obtained from a 50-member ensemble of reanalyses driven, COSMO-CLM simulations.

Non-negligible baroclinicity, indicated by large vertical wind shear, characterizes the early stages of the simulated cyclones. As these undergo a warm seclusion-like process, the initial thermal asymmetries and vertical tilt are reduced while a warm core builds upward from the lower troposphere in a manner consistent with the baroclinically-induced pathway to tropical cyclogenesis (Bosart and Bartlo 1991; Davis and Bosart 2003)

In the transitioning cyclones, significantly stronger convection is present in the mid-upper troposphere, resulting in larger release of latent heat by condensation. At the transition, the tropospheric wind shear declines in both composites below 10 m/s, in agreement with the empirical thresholds calculated for TCs of 15 m/s (DeMaria et al. 2001) and 10-12 m/s (Gallina and Velden 2002), and within the 4-29 m/s range calculated for medicanes by Tous et al. (2013). Although the medicanes feature on average a more pronounced shear reduction, even in the non-transitioning cyclones the shear weakens to favorable values. This differs from the findings of previous studies on tropical transitions (Davis and Bosart 2003) and on the intensification of TCs (Hendricks et al. 2010; Kaplan et al. 2010). Just like baroclinically-induced TCs (Davis and Bosart 2003) and a subset of all North Atlantic TCs (Bracken and Bosart 2000), medicanes seem to benefit from an initial moderate degree of shear. A significant, positive difference over a 5-period preceding TT suggests that upper-level wind divergence can be relevant in supporting convection during the tropical transition, as also proposed by Chaboureau et al. (2012). Furthermore, the correlation analysis indicates that a compensation exists between wind shear and divergence, as the detrimental effects of high wind shear might be counteracted by an increased forcing on vertical motions.

Enhanced surface latent and sensible heat fluxes characterize only the post-transition stage, consistent with the WISHE mechanism sustaining the intensification of medicanes during their mature stage (Emanuel 2005; Fita et al. 2007). The layer between 600 and 850 hPa features significantly higher relative humidity: somewhat in contrast with previous studies (Tous and Romero 2011; Tous et al. 2013), enhanced mid-tropospheric relative humidity emerges here as a distinctive feature of the transitioning cyclones. Higher mid-tropospheric relative humidity, exhibiting azimuthal asymmetries, has been also found in the near-environment of rapidly intensifying hurricanes (Hendricks et al. 2010; Wu et al. 2012; Rios-Berrios et al. 2015). As suggested by Rios-Berrios et al. (2015), a moister mid-troposphere would better support sustained convection, preventing dry air entrainment as well as reducing the stabilizing effects of convective downdrafts.

Within the limitations posed by a single case study, these findings provide a more detailed characterization of the meteorological environment in which tropical transitions can occur in the Mediterranean Basin. Further investigations are required in order to assess the causal relationships between the observed differences and the transition process. Nevertheless, the results presented in this study might contribute to the current understanding of medicanes and also prove relevant for the general community dealing with baroclinically-induced tropical cyclogeneses.

Acknowledgments. The computational resources were made available by the German Climate Computing Center (DKRZ). The authors would like to acknowledge the Helmholtz graduate research school GeoSim for funding this research. R.K.'s research has been partially funded by Deutsche Forschungsgemeinschaft (DFG) through grant CRC 1114/C06. E.M. would like to thank Daniel Befort for his help in setting up the RCM, Bijan Fallah, Emmanuele Russo, Nico Becker and Walter Acevedo for their fruitful comments and Beatrice Magistro for her constant support.

References

Akhtar, N., J. Brauch, A. Dobler, K. Branger, and B. Ahrens, 2014: Medicanes in an ocean-atmosphere coupled regional climate model. *Nat. Hazards Earth Syst. Sci.*, **14 (8)**, 2189–2201, URL http://www.nat-hazards-earth-syst-sci.net/14/2189/2014/.

Bengtsson, L., K. I. Hodges, M. Esch, N. Keenlyside, L. Kornblueh, J. LUO, and T. Yamagata, 2007: How may tropical cyclones change in a warmer climate? *Tellus A*, **59 (4)**, 539–561.

Bosart, L. F., and J. A. Bartlo, 1991: Tropical storm formation in a baroclinic environment. *Mon. Wea. Rev.*, **119 (8)**, 1979–2013, doi:10.1175/1520-0493(1991)119⟨1979:TSFIAB⟩2.0.CO;2, URL http://dx.doi.org/10.1175/1520-0493(1991)119⟨1979:TSFIAB⟩2.0.CO;2.

Bracken, W. E., and L. F. Bosart, 2000: The role of synoptic-scale flow during tropical cyclogenesis over the north atlantic ocean. *Mon. Wea. Rev.*, **128 (2)**, 353–376, doi: 10.1175/1520-0493(2000)128⟨0353:TROSSF⟩2.0.CO;2, URL http://journals.ametsoc.org/doi/abs/10.1175/1520-0493%282000%29128%3C0353%3ATROSSF%3E2.0.CO%3B2.

Brown, B. R., and G. J. Hakim, 2015: Sensitivity of intensifying atlantic hurricanes to vortex structure. *Quarterly Journal of the Royal Meteorological Society*, **141**, 2538–2551.

Catto, J. L., L. C. Shaffrey, and K. I. Hodges, 2010: Can climate models capture the structure of extratropical cyclones? *J. Climate*, **23 (7)**, 1621–1635.

Cavicchia, L., and H. von Storch, 2012: The simulation of medicanes in a high-resolution regional climate model. *Clim. Dyn.*, **39 (9-10)**, 2273–2290.

Cavicchia, L., H. von Storch, and S. Gualdi, 2014: A long-term climatology of medicanes. *Clim. Dyn.*, **43 (5-6)**, 1183–1195.

Chaboureau, J.-P., F. Pantillon, D. Lambert, E. Richard, and C. Claud, 2012: Tropical transition of a mediterranean storm by jet crossing. *Q.J.R. Meteorol. Soc.*, **138 (664)**, 596–611, URL http://dx.doi.org/10.1002/qj.960.

Claud, C., B. Alhammoud, B. M. Funatsu, and J.-P. Chaboureau, 2010: Mediterranean hurricanes: large-scale environment and convective and precipitating areas from satellite microwave observations. *Nat. Hazards Earth Syst. Sci.*, **10 (10)**, 2199–2213, URL http://www.nat-hazards-earth-syst-sci.net/10/2199/2010/.

Davis, C. A., and L. F. Bosart, 2003: Baroclinically induced tropical cyclogenesis. *Mon. Wea. Rev.*, **131 (11)**, 2730–2747, doi:10.1175/1520-0493(2003)131⟨2730:BITC⟩2.0.CO;2, URL http://dx.doi.org/10.1175/1520-0493(2003)131⟨2730:BITC⟩2.0.CO;2.

Davis, C. A., and L. F. Bosart, 2004: The tt problem: Forecasting the tropical transition of cyclones. *Bull. Amer. Meteor. Soc.*, **85 (11)**, 1657–1662, doi:10.1175/BAMS-85-11-1657, URL http://dx.doi.org/10.1175/BAMS-85-11-1657.

Davolio, S., M. M. Miglietta, A. Moscatello, F. Pacifico, A. Buzzi, and R. Rotunno, 2009: Numerical forecast and analysis of a tropical-like cyclone in the ionian sea. *Nat. Hazards Earth Syst. Sci.*, **9 (2)**, 551–562, URL http://www.nat-hazards-earth-syst-sci.net/9/551/2009/.

Dee, D. P., and Coauthors, 2011: The era-interim reanalysis: configuration and performance of the data assimilation system. *Q.J.R. Meteorol. Soc.*, **137 (656)**, 553–597, URL http://dx.doi.org/10.1002/qj.828.

DeMaria, M., J. A. Knaff, and B. H. Connell, 2001: A tropical cyclone genesis parameter for the tropical atlantic. *Wea. Forecasting*, **16 (2)**, 219–233, doi:10.1175/1520-0434(2001)016⟨0219:ATCGPF⟩2.0.CO;2, URL http://dx.doi.org/10.1175/1520-0434(2001)016⟨0219:ATCGPF⟩2.0.CO;2.

Emanuel, K., 2005: Genesis and maintenance of ”mediterranean hurricanes”. *Adv. Geosci.*, **2**, 217–220, URL http://www.adv-geosci.net/2/217/2005/.

Emanuel, K. A., 1986: An air-sea interaction theory for tropical cyclones. part i: Steady-state maintenance. *J. Atmos. Sci.*, **43 (6)**, 585–605, doi:10.1175/1520-0469(1986)043⟨0585:AASITF⟩2.0.CO;2, URL http://dx.doi.org/10.1175/1520-0469(1986)043⟨0585:AASITF⟩2.0.CO;2.

Fita, L., R. Romero, A. Luque, K. Emanuel, and C. Ramis, 2007: Analysis of the environments of seven mediterranean tropical-like storms using an axisymmetric, nonhydrostatic, cloud resolving model. *Nat. Hazards Earth Syst. Sci.*, **7 (1)**, 41–56, URL http://www.nat-hazards-earth-syst-sci.net/7/41/2007/.

Frank, W. M., 1977: The structure and energetics of the tropical cyclone i. storm structure. *Mon. Wea. Rev.*, **105 (9)**, 1119–1135.

Gallina, G. M., and C. S. Velden, 2002: 3c. 5 environmental vertical wind shear and tropical cyclone intensity change utilizing enhanced satellite derived wind information. *Atlantic*, **58**, 12.

Hart, R. E., 2003: A cyclone phase space derived from thermal wind and thermal asymmetry. *Mon. Wea. Rev.*, **131 (4)**, 585–616, doi:10.1175/1520-0493(2003)131⟨0585:ACPSDF⟩2.0.CO;2, URL http://dx.doi.org/10.1175/1520-0493(2003)131⟨0585:ACPSDF⟩2.0.CO;2.

Hendricks, E. A., M. S. Peng, B. Fu, and T. Li, 2010: Quantifying environmental control on tropical cyclone intensity change. *Mon. Wea. Rev.*, **138 (8)**, 3243–3271, doi:10.1175/2010MWR3185.1, URL http://dx.doi.org/10.1175/2010MWR3185.1.

Hulme, A. L., and J. Martin, 2006: The role of the occlusion process in the extratropical-to-tropical transition of atlantic hurricane karen. *27th Conference on Hurricanes and Tropical Meteorology*.

Hulme, A. L., and J. E. Martin, 2009a: Synoptic- and frontal-scale influences on tropical transition events in the atlantic basin. part i: A six-case survey. *Mon. Wea. Rev.*, **137 (11)**, 3605–3625, doi:10.1175/2009MWR2802.1, URL http://dx.doi.org/10.1175/2009MWR2802.1.

Hulme, A. L., and J. E. Martin, 2009b: Synoptic- and frontal-scale influences on tropical transition events in the atlantic basin. part ii: Tropical transition of hurricane karen. *Mon. Wea. Rev.*, **137 (11)**, 3626–3650, doi:10.1175/2009MWR2803.1, URL http://dx.doi.org/10.1175/2009MWR2803.1.

Jones, S. C., and Coauthors, 2003: The extratropical transition of tropical cyclones: Forecast challenges, current understanding, and future directions. *Wea. Forecasting*, **18 (6)**, 1052–1092, doi:10.1175/1520-0434(2003)018⟨1052:TETOTC⟩2.0.CO;2, URL http://dx.doi.org/10.1175/1520-0434(2003)018⟨1052:TETOTC⟩2.0.CO;2.

Kaplan, J., M. DeMaria, and J. A. Knaff, 2010: A revised tropical cyclone rapid intensification index for the atlantic and eastern north pacific basins. *Wea. Forecasting*, **25 (1)**, 220–241, doi:10.1175/2009WAF2222280.1, URL http://dx.doi.org/10.1175/2009WAF2222280.1.

Lagouvardos, K., V. Kotroni, D. Jovic, S Nickovic, G. Kallos, and C. J. Tremback, 1999: Observations and model simulations of a winter sub-synoptic vortex over the central mediterranean. *Meteorological Applications*, **6 (04)**, 371–383, doi:null, URL http://dx.doi.org/10.1017/S1350482799001309.

McBride, J. L., and R. Zehr, 1981: Observational analysis of tropical cyclone formation. part ii: Comparison of non-developing versus developing systems. *J. Atmos. Sci.*, **38 (6)**, 1132–1151, doi:10.1175/1520-0469(1981)038⟨1132:OAOTCF⟩2.0.CO;2, URL http://dx.doi.org/10.1175/1520-0469(1981)038⟨1132:OAOTCF⟩2.0.CO;2.

McTaggart-Cowan, R., T. J. Galarneau, L. F. Bosart, and J. A. Milbrandt, 2009a: Development and tropical transition of an alpine lee cyclone. part i: Case analysis and evaluation of numerical guidance. *Mon. Wea. Rev.*, **138 (6)**, 2281–2307, doi:10.1175/2009MWR3147.1, URL http://dx.doi.org/10.1175/2009MWR3147.1.

McTaggart-Cowan, R., T. J. Galarneau, L. F. Bosart, and J. A. Milbrandt, 2009b: Development and tropical transition of an alpine lee cyclone. part ii: Orographic influence on the development pathway. *Mon. Wea. Rev.*, **138 (6)**, 2308–2326, doi:10.1175/2009MWR3148.1, URL http://dx.doi.org/10.1175/2009MWR3148.1.

McTaggart-Cowan, R., T. J. Galarneau, L. F. Bosart, R. W. Moore, and O. Martius, 2012: A global climatology of baroclinically influenced tropical cyclogenesis*. *Mon. Wea. Rev.*, **141 (6)**, 1963–1989, doi:10.1175/MWR-D-12-00186.1, URL http://dx.doi.org/10.1175/MWR-D-12-00186.1.

Miglietta, M. M., S. Laviola, A. Malvaldi, D. Conte, V. Levizzani, and C. Price, 2013: Analysis of tropical-like cyclones over the mediterranean sea through a combined modeling and satellite approach. *Geophys. Res. Lett.*, **40 (10)**, 2400–2405, URL http://dx.doi.org/10.1002/grl.50432.

Moscatello, A., M. Marcello Miglietta, and R. Rotunno, 2008a: Observational analysis of a mediterranean ”hurricane” over south-eastern italy. *Weather*, **63 (10)**, 306–311, URL http://dx.doi.org/10.1002/wea.231.

Moscatello, A., M. M. Miglietta, and R. Rotunno, 2008b: Numerical analysis of a mediterranean ”hurricane” over southeastern italy. *Mon. Wea. Rev.*, **136 (11)**, 4373–4397, doi:10.1175/2008MWR2512.1, URL http://dx.doi.org/10.1175/2008MWR2512.1.

Pantillon, F. P., J.-P. Chaboureau, P. J. Mascart, and C. Lac, 2012: Predictability of a mediterranean tropical-like storm downstream of the extratropical transition of hurricane helene (2006). *Mon. Wea. Rev.*, **141 (6)**, 1943–1962, doi:10.1175/MWR-D-12-00164.1, URL http://dx.doi.org/10.1175/MWR-D-12-00164.1.

Paterson, L. A., B. N. Hanstrum, N. E. Davidson, and H. C. Weber, 2005: Influence of environmental vertical wind shear on the intensity of hurricane-strength tropical cyclones in the australian region. *Mon. Wea. Rev.*, **133 (12)**, 3644–3660, doi:10.1175/MWR3041.1, URL http://dx.doi.org/10.1175/MWR3041.1.

Pytharoulis, I., G. C. Craig, and S. P. Ballard, 2000: The hurricane-like mediterranean cyclone of january 1995. *Met. Apps*, **7 (3)**, 261–279, URL http://dx.doi.org/10.1017/S1350482700001511.

Reale, O., and R. Atlas, 2001: Tropical cyclone-like vortices in the extratropics: Observational evidence and synoptic analysis. *Wea. Forecasting*, **16 (1)**, 7–34, doi:10.1175/1520-0434(2001)016⟨0007:TCLVIT⟩2.0.CO;2, URL http://dx.doi.org/10.1175/1520-0434(2001)016⟨0007:TCLVIT⟩2.0.CO;2.

Reed, R., Y.-H. Kuo, M. Albright, K. Gao, Y.-R. Guo, and W. Huang, 2001: Analysis and modeling of a tropical-like cyclonein the mediterranean sea. *Meteorology and Atmospheric Physics*, **76 (3-4)**, 183–202.

Rios-Berrios, R., R. D. Torn, and C. A. Davis, 2015: An ensemble approach to investigate tropical cyclone intensification in sheared environments. part i: Katia (2011). *J. Atmos. Sci.*, **8**, doi:10.1175/JAS-D-15-0052.1, URL http://dx.doi.org/10.1175/JAS-D-15-0052.1.

Rockel, B., A. Will, and A. Hense, 2008: The regional climate model cosmo-clm (cclm). *Meteorologische Zeitschrift*, **17 (4)**, 347–348.

Rotunno, R., and K. A. Emanuel, 1987: An air-sea interaction theory for tropical cyclones. part ii: Evolutionary study using a nonhydrostatic axisymmetric numerical model. *J. Atmos. Sci.*, **44 (3)**, 542–561, doi:10.1175/1520-0469(1987)044⟨0542:AAITFT⟩2.0.CO;2, URL http://dx.doi.org/10.1175/1520-0469(1987)044⟨0542:AAITFT⟩2.0.CO;2.

Shapiro, M. A., and D. A. Keyser, 1990: *Fronts, jet streams, and the tropopause*. US Department of Commerce, National Oceanic and Atmospheric Administration, Environmental Research Laboratories, Wave Propagation Laboratory.

Tiedtke, M., 1989: A comprehensive mass flux scheme for cumulus parameterization in large-scale models. *Mon. Wea. Rev.*, **117 (8)**, 1779–1800.

Tous, M., and R. Romero, 2011: Medicanes: cataloguing criteria and exploration of meteorological environments. *Tethys*, **8**, 53–61.

Tous, M., and R. Romero, 2013: Meteorological environments associated with medicane development. *Int. J. Climatol.*, **33 (1)**, 1–14.

Tous, M., R. Romero, and C. Ramis, 2013: Surface heat fluxes influence on medicane trajectories and intensification. *Atm. Res.*, **123**, 400–411.

Trigo, I. F., T. D. Davies, and G. R. Bigg, 1999: Objective climatology of cyclones in the mediterranean region. *J. Climate*, **12 (6)**, 1685–1696, doi:10.1175/1520-0442(1999)012⟨1685:OCOCIT⟩2.0.CO;2, URL http://dx.doi.org/10.1175/1520-0442(1999)012⟨1685:OCOCIT⟩2.0.CO;2.

Uppala, S. M., and Coauthors, 2005: The era-40 reanalysis. *Q. J. R. Meteorol. Soc.*, **131 (612)**, 2961–3012.

Wu, L., and Coauthors, 2012: Relationship of environmental relative humidity with north atlantic tropical cyclone intensity and intensification rate. *Geophys. Res. Lett.*, **39 (20)**, 1–8.

LIST OF TABLES

TABLE 1. Summary of the area-averaged parameters analyzed for the MED (left) and NONMED (right) composites at TT-12, TT and their average over the 12 hours preceeding the transition.

	TT-12h	TT	$\langle TT \rangle_0^{-12}$
	MED | NONMED	MED | NONMED	MED | NONMED
$\langle 600-850 \rangle$ hPa RH (%)	85.5 | 80.3	81.5 | 76.9	84.4 | 79.4
300-850 hPa Shear(m/s)	24.5 | 17.7	8.5 | 6.9	14.7 | 11.0
300 hPa Divergence (x10^{-5} 1/s)	2.4 | 1.7	1.3 | 0.4	2.3 | 1.5
Latent Heat Flux (W/m^2)	144.9 | 131.3	278.9 | 233.9	189.9 | 184.7
Sensible Heat Flux (W/m^2)	42.8 | 38.4	112.4 | 91.9	66.7 | 67.7

LIST OF FIGURES

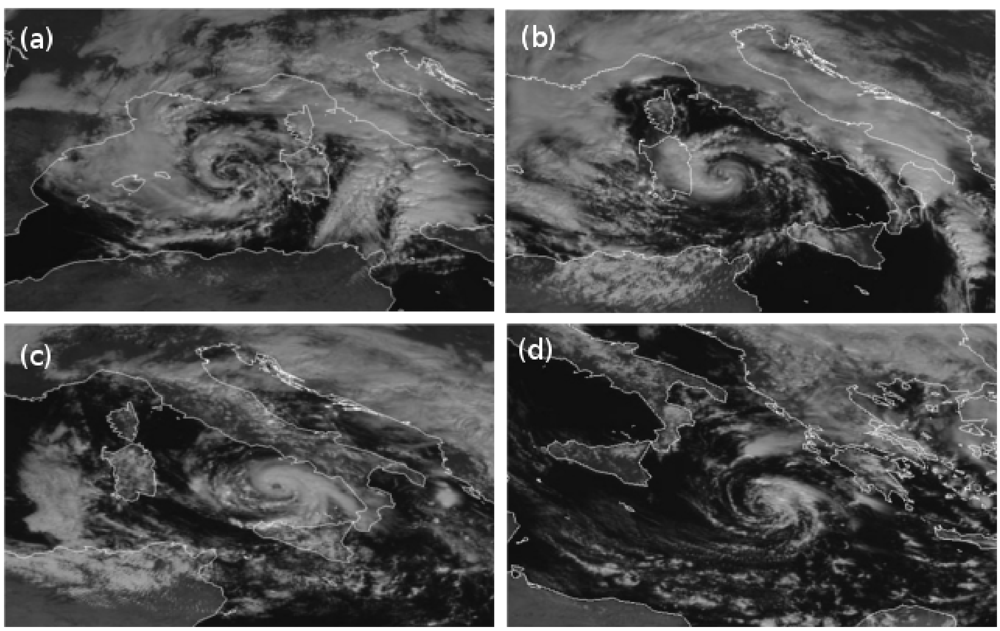

FIG. 1. METEOSAT-5 0.6 μm visible channel imagery of the October 1996 medicane: at a) 1000 UTC, October 7th; b) 1030 UTC, October 8th; c) 1030 UTC, October 9th; d) 1030 UTC, October 10th.

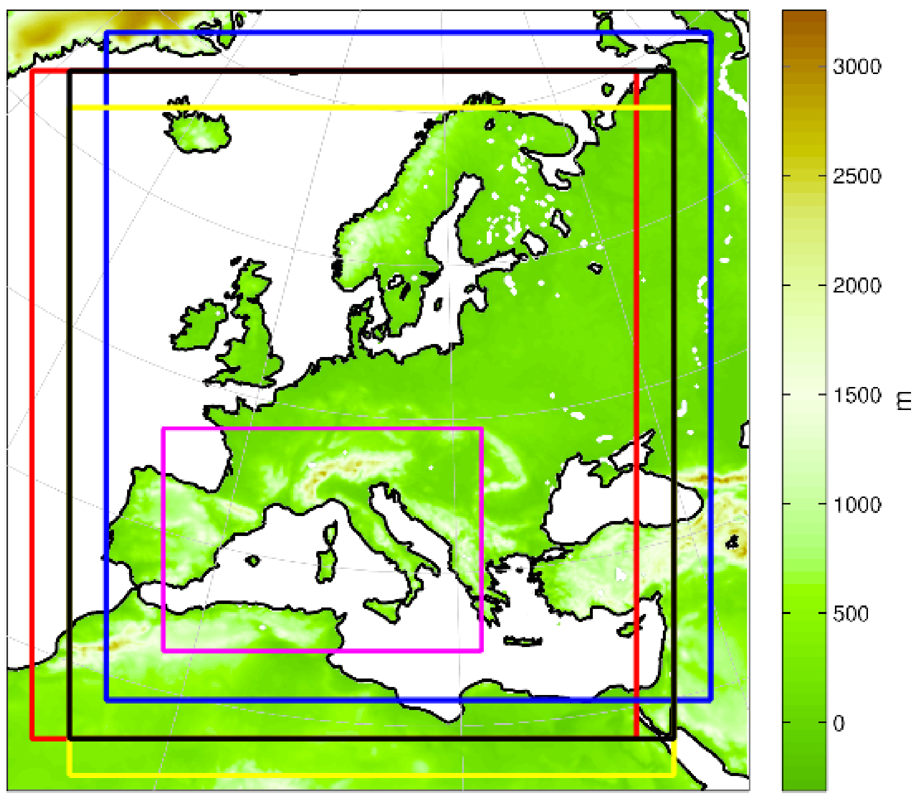

FIG. 2. a) Elevation map and simplified example of the *domain shifting* set up used on the first downscaling: the shifted domains are ORIG (black), West (red), North-West (blue), South (yellow). In each domain a second, nested grid (magenta) is employed for the second downscaling.

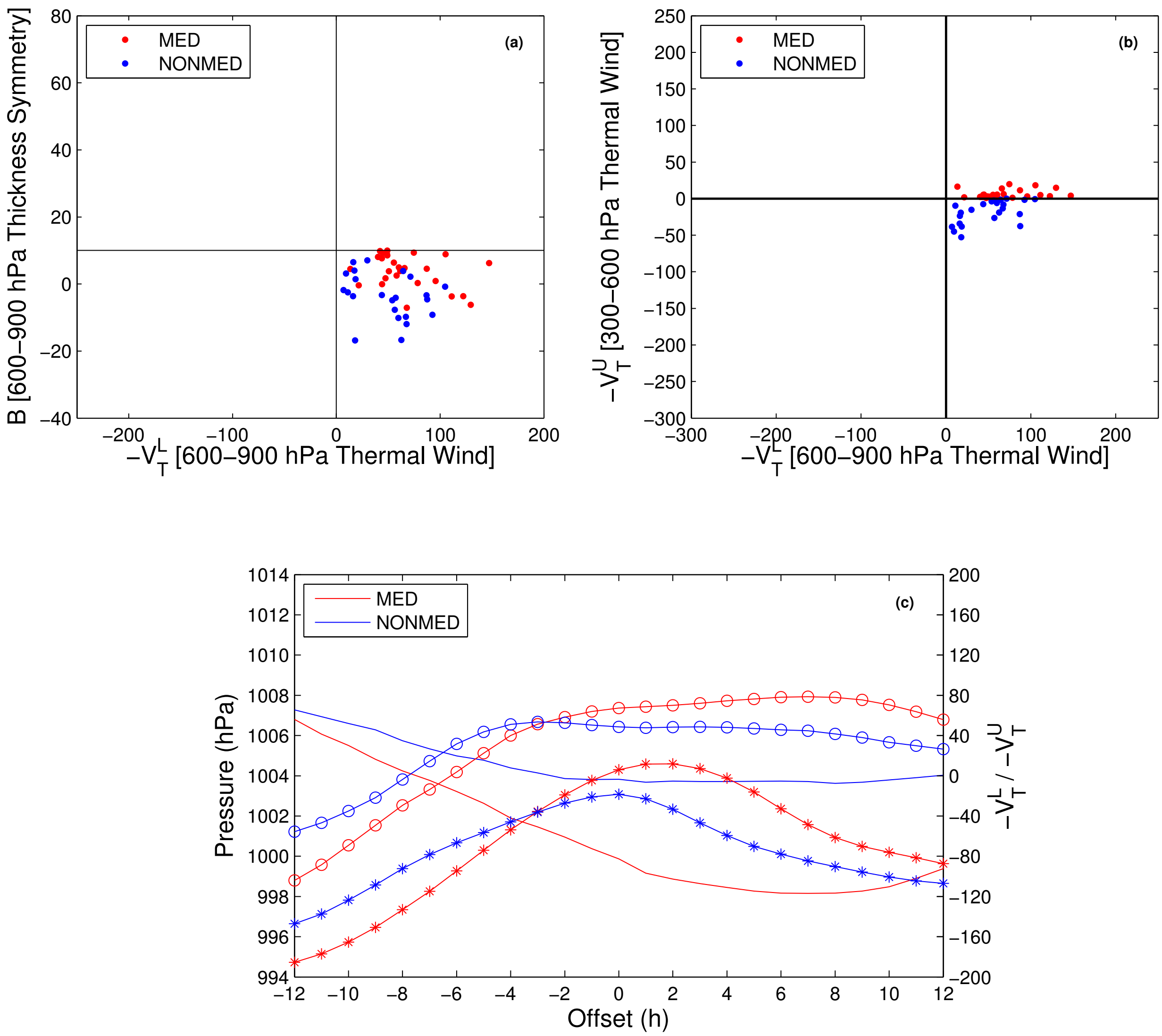

FIG. 3. Cyclone-phase space diagrams at TT time: (a) -V_T^L vs. B, (b) -V_T^L vs. -V_T^U. Each point represents a composite member. (c) Composite time series of SLP minimum (solid lines - values refer to left-hand axis) and phase space warm core metrics (dashed line with circular markers for -V_T^L, with cross markers for -V_T^U - values refer to right-hand axis).

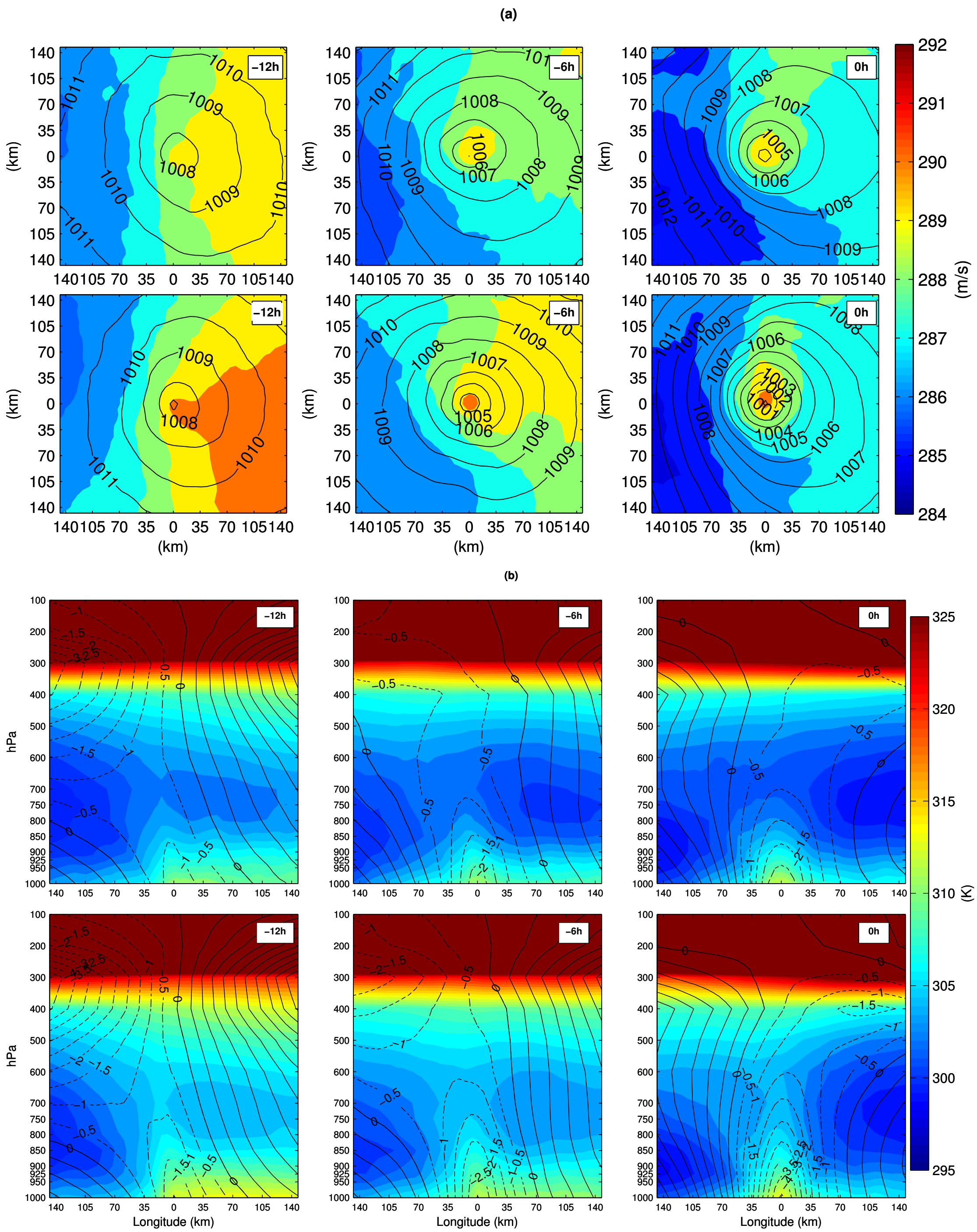

551 FIG. 4. (a) 900 hPa potential tempetature (colors) and SLP (contours every hPa) for NONMED (top) and MED (bottom) at -12h, -6h, +0h. (b) Longitudinal cross sections through the composite centre of equivalent potential temperature (colors) and geopotential height anomaly (contoured every 0.5 gpdm - dashed when negative) at -12h, -6h, +0h.

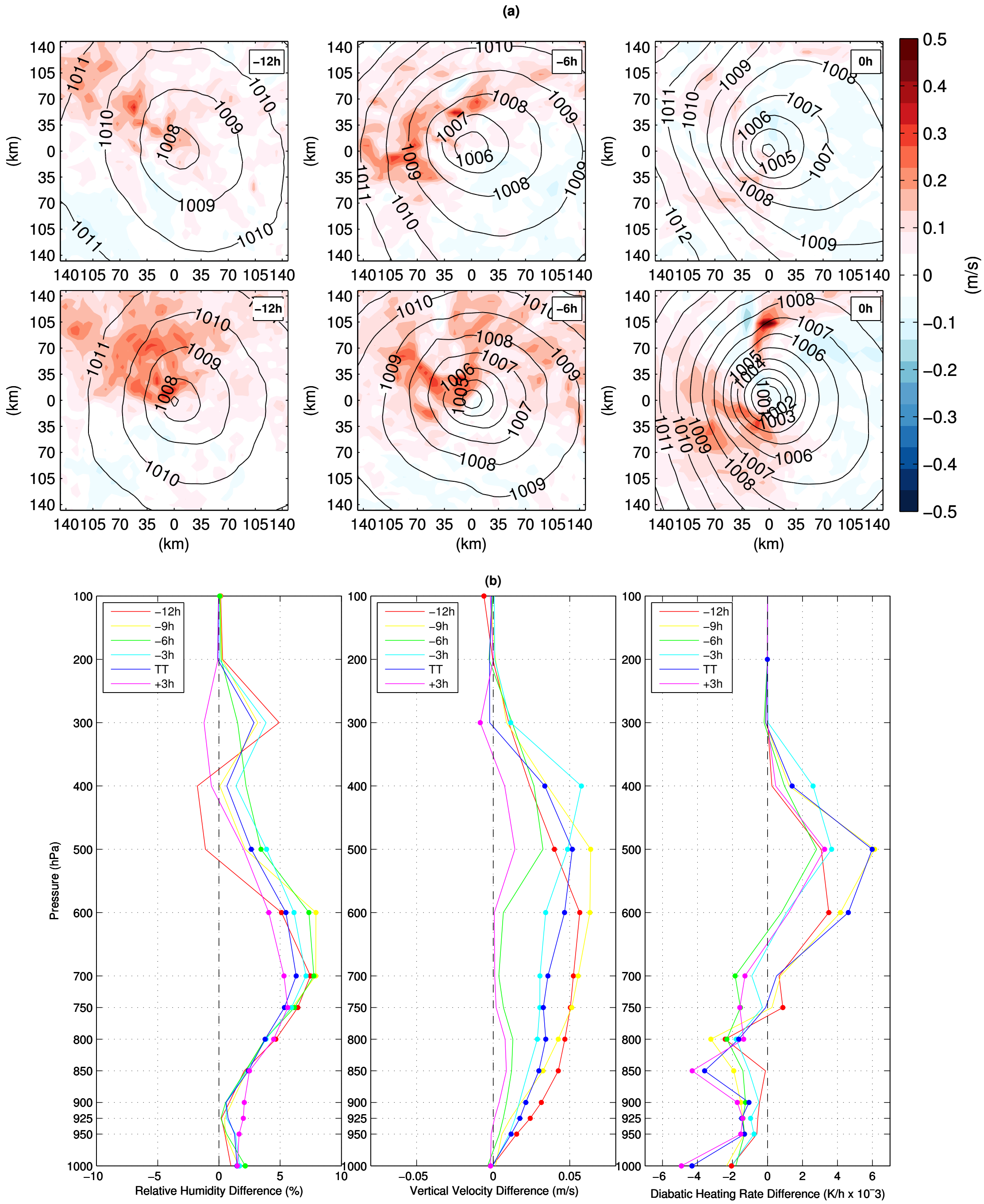

FIG. 5. (a) 500 hPa vertical velocity (colors) and SLP (contours every hPa) for NONMED (top) and MED (bottom) at -12h, -6h, +0h. (b): Vertical profiles of area-averaged relative humidity (left), vertical velocity (middle) and diabatic heating rate (right) differences (MED-NONMED) at -12h, -9h, -6h, -3h, TT=0h, +3h offsets. Vertical velocities and diabatic heating rate are averaged within 70 km from the composite centre. Circular markers indicate where the difference is significant at the 95% condifence interval.

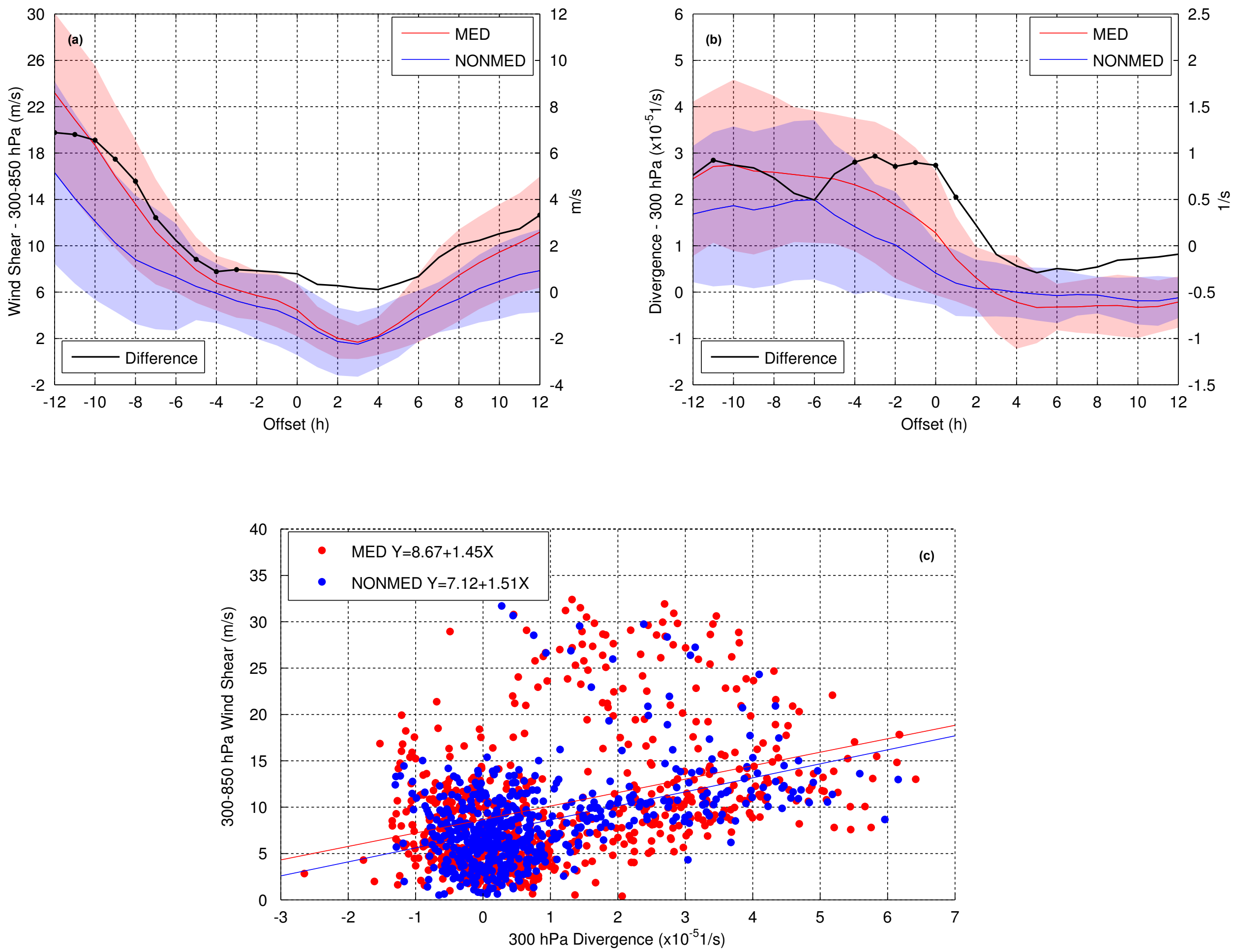

FIG. 6. Composite time series for MED and NONMED of area-averaged: (a) 300-850 hPa wind shear and (b) 300 hPa wind divergence and corresponding differences (black line - refer to right hand axis). Circular markers indicate a statistically significant difference at the 95% confidence interval. Shading denotes $\pm\sigma$. (c) Scatter plot of 300-850 hPa and 300 hPa wind divergence for MED and NONMED composites and corresponding linear fits whose equations are provided in the legend box.

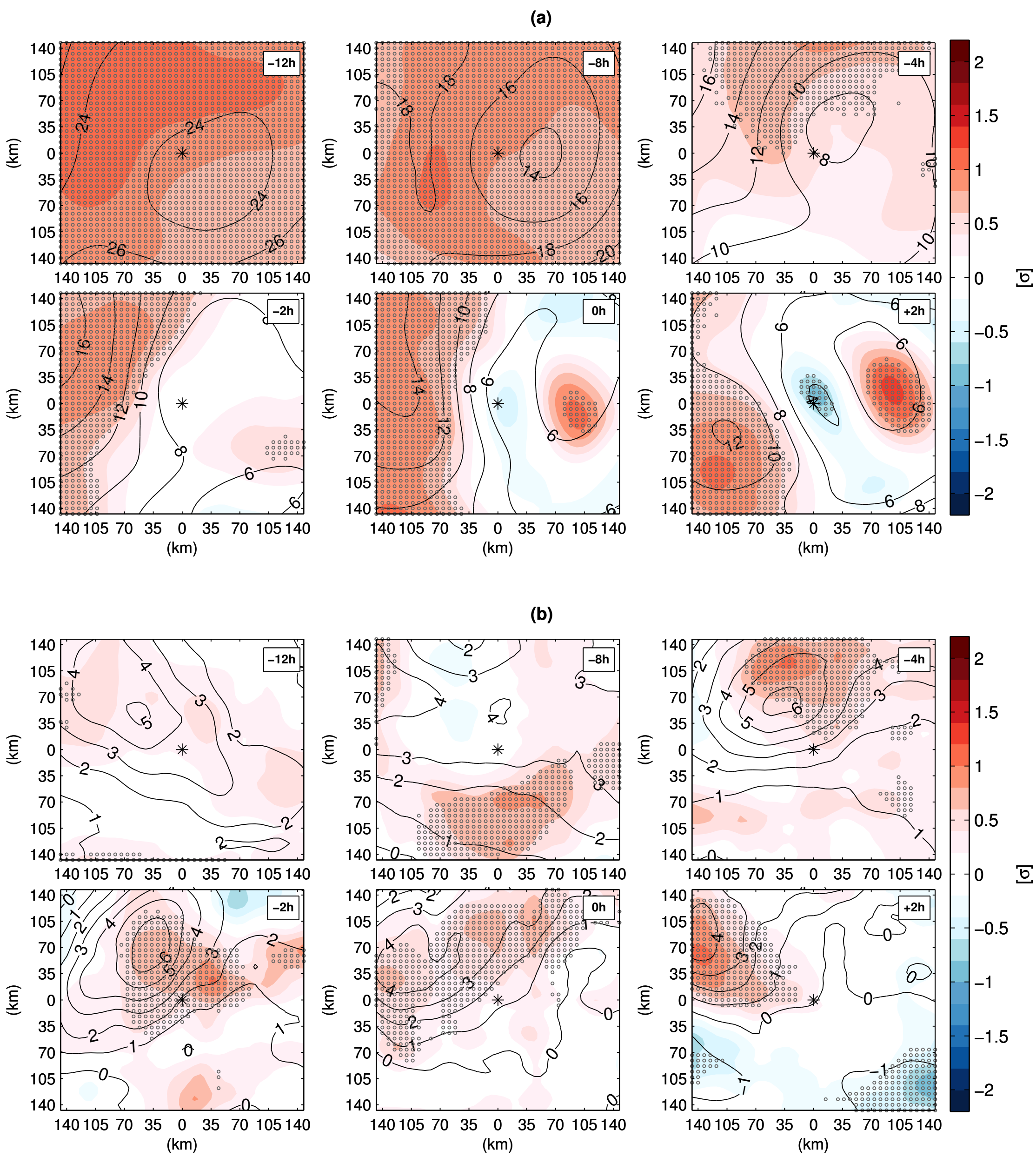

FIG. 7. Ensemble mean (contours) and normalized composite difference (colors) at -12h, -8h, -4h, -2h, 0, +2h. (a) 300-850 hPa wind shear; (b) 300 hPa wind divergence (contours every 1x10^{-5} $1/s$). Grey dots indicate where the difference is statistically significant at the 95% confidence interval.

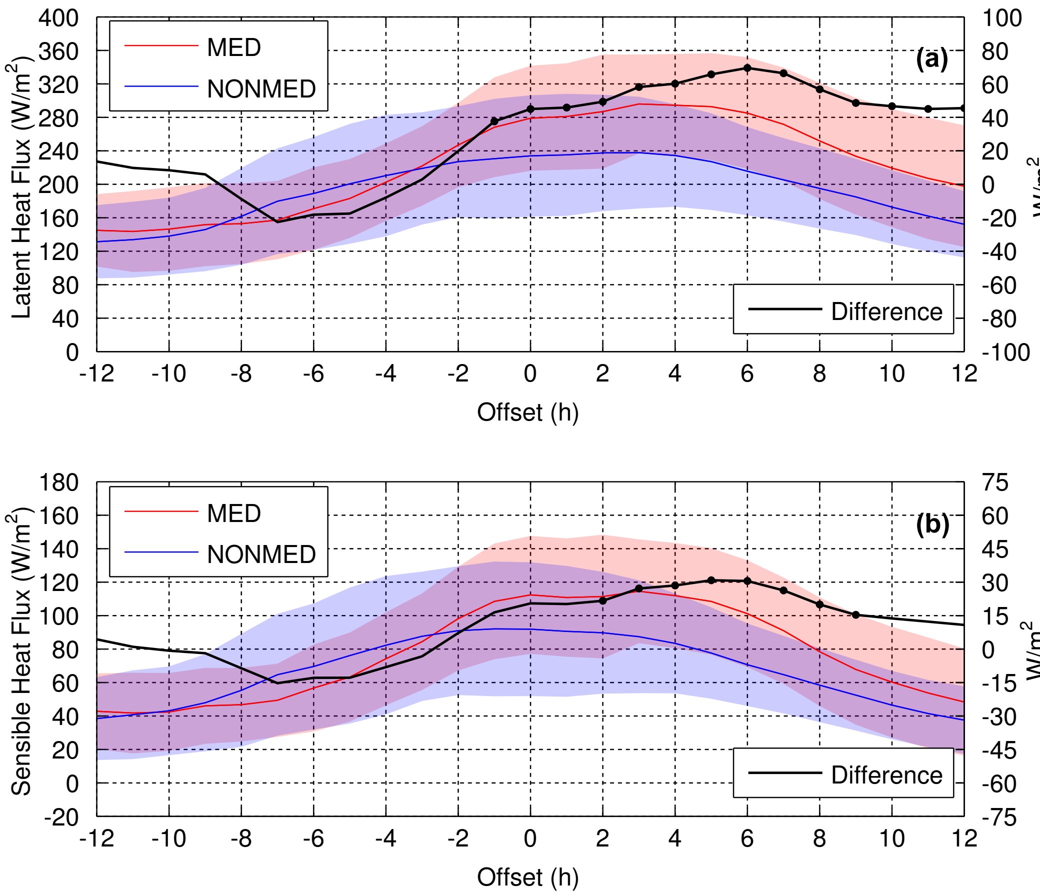

568 FIG. 8. Composite time series for MED and NONMED of area-averaged: (a) latent heat and (b) sensible heat fluxes and corresponding differences (black line - refer to right hand axis). Circular markers indicate a statistically significant difference at the 95% confidence interval. Shading denotes $\pm\sigma$.

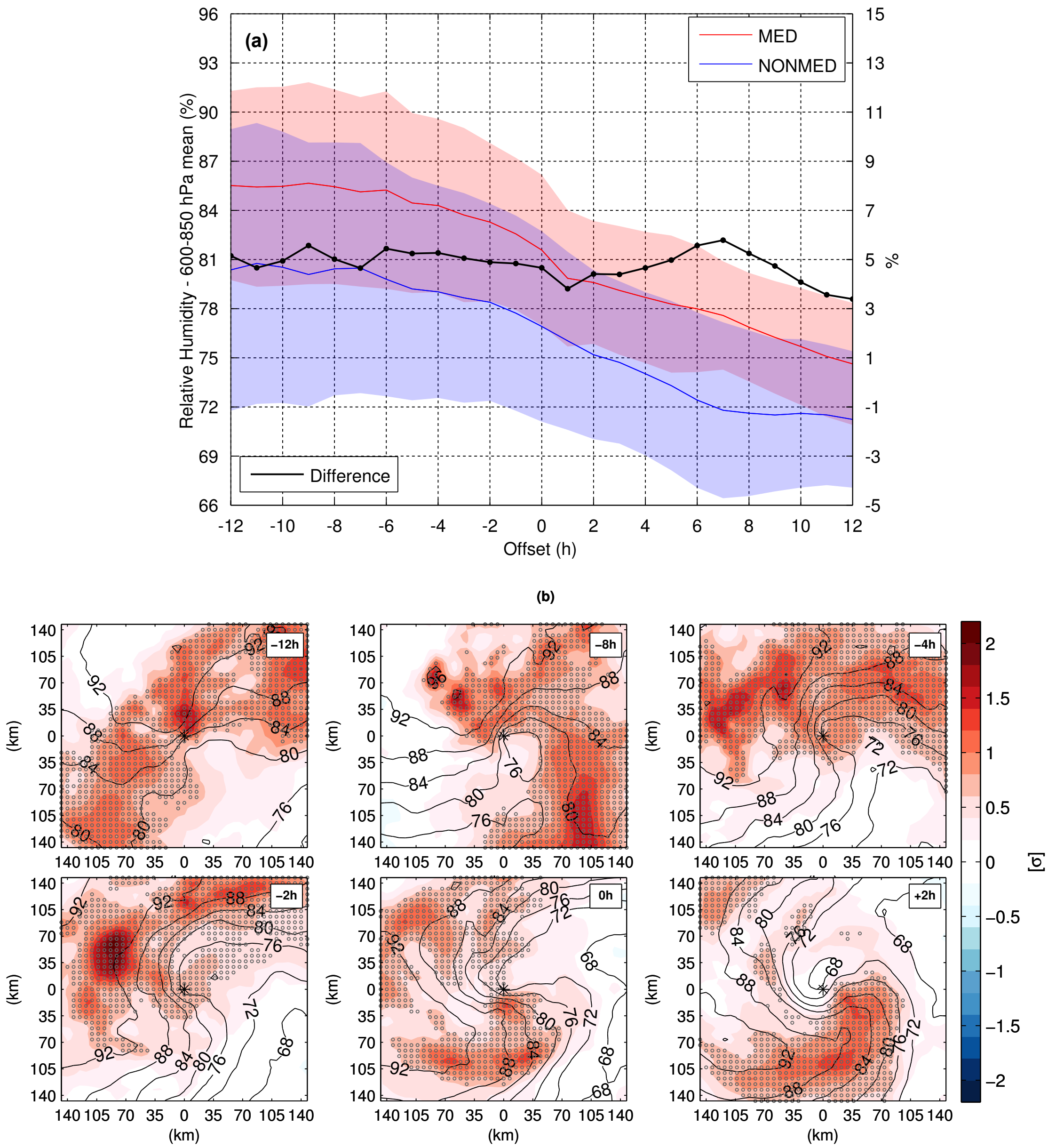

FIG. 9. (a) Composite time series for MED and NONMED of area-averaged 600-850 hPa mean relative humidity and corresponding differences (black line - refer to right hand axis). Circular markers indicate a statistically significant difference at the 95% confidence level. Shading denotes $\pm\sigma$. (b) Ensemble mean 600-850 hPa mean relative humidity (contoured every 4%) and normalized composite difference (colors) at -12h, -8h, -4h, -2h, 0, +2h. Grey dots indicate where the difference is statistically significant at the 95% confidence interval.

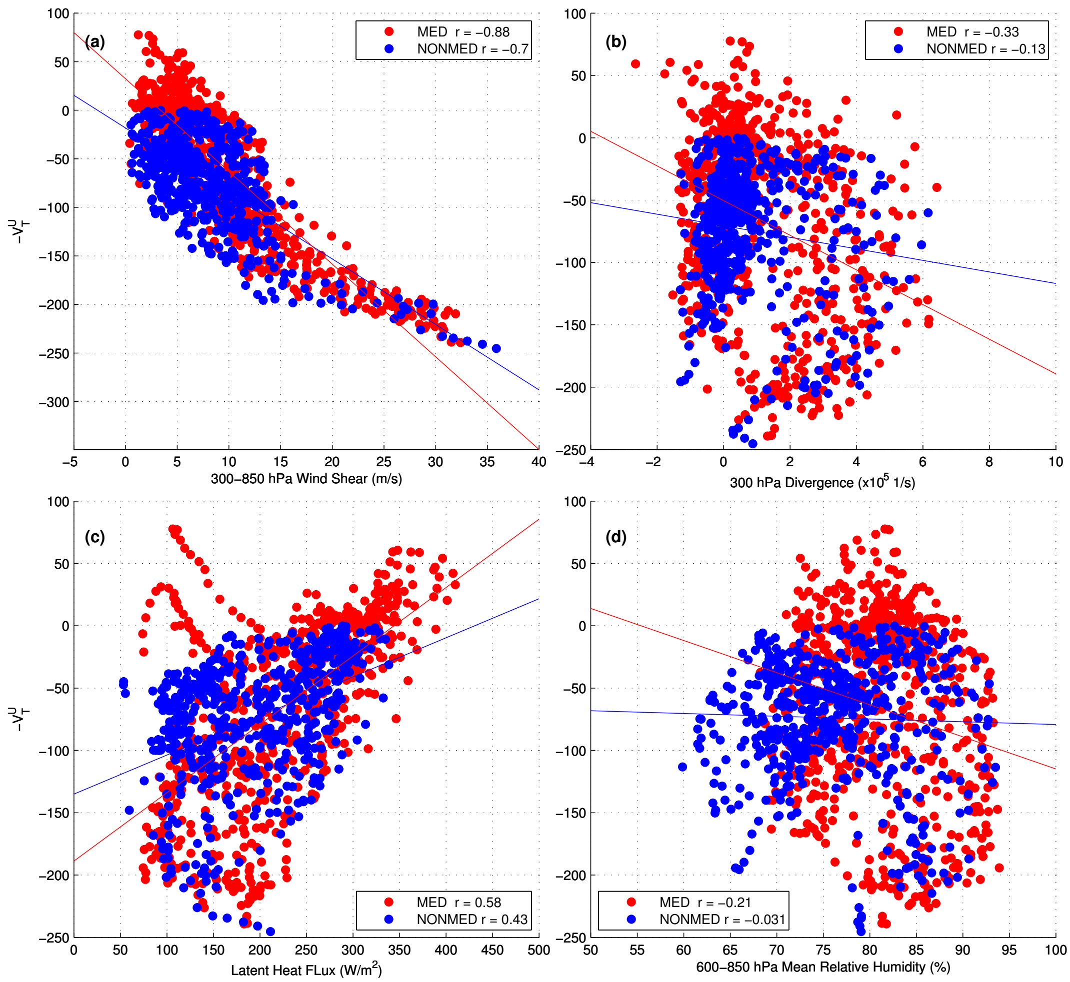

577 FIG. 10. Scatter plots of area averaged 300-850 hPa wind shear (a), 300 hPa divergence (b), latent heat flux
578 (c), 600-850 hPa mean relative humidity (d) against the cyclone phase space upper-tropospheric warm core
579 metric -V_T^U. Each set of points is linearly fitted, the corresponding Pearson correlation coefficients are provided
580 in the legend boxes.